Received: 12 January 2021 | Revised: 6 May 2021 | Accepted: 7 May 2021

DOI: 10.1002/jrs.6147

SPECIAL ISSUE - RESEARCH ARTICLE

Journal of RAMAN SPECTROSCOPY WILEY

Raman spectra of the Markovka chondrite (H4)

Sergey Voropaev[1] | **Ute Böttger**[2] | **Sergey G. Pavlov**[2] | **Franziska Hanke**[2] | **Dmitri Petukhov**[3]

[1]Laboratory of Carbon Geochemistry, GEOKHI RAS, Moscow, Russia

[2]Institute of Optical Sensor Systems, German Aerospace Center (DLR), Berlin, Germany

[3]Analytical Centre, Moscow State University, Moscow, Russia

Correspondence
Sergey Voropaev, Laboratory of Carbon Geochemistry, GEOKHI RAS, Kosygina str. 19, Moscow 119991, Russia.
Email: voropaev@geokhi.ru

Funding information
Russian Science Foundation, Grant/Award Number: 21-17-00120

Abstract

Raman spectroscopy and scanning electron microscopy methods were used to study the fragment of the Markovka (H4 chondrite) meteorite. A characteristic set of silicate minerals (olivine and pyroxene), oxides and hydroxides (maghemite and goethite), troilite, and carbonates (aragonite) was determined. The structural features revealed by Raman spectroscopy allow us to draw important conclusions on thermal history of the parent body including both the temperature experienced by the rock on the parent body and their cooling rate as well as the constraints on the size of the parent body and the Mg composition of the assumed fluid.

KEYWORDS

asteroid, carbonates, chondrite, meteorite, thermal history

1 | INTRODUCTION

Chondrite meteorites, which are generally accepted to be accreted from very pristine materials of the solar system, are grouped into three petrologic classes: carbonaceous, ordinary, and enstatite chondrites. On the basis of their iron and other metal contents, the ordinary chondrites are further subdivided into three chemical classes: H, L, and LL, and Types 3, 4, 5, and 6, depending on the intensity of thermal metamorphism: Type 3 is unheated, whereas Types 4 through 6 have been progressively heated.[1,2] It was shown that Raman spectroscopy can provide valuable information about mineral composition and thermal history of ordinary and carbonaceous chondrites.[3–7] Freshly fallen meteorites are particularly valuable for the planetary science community because they typically contain very old (~4.55 billion years old) material from the early solar nebula that has not been altered by terrestrial weathering. Thus, they can provide scientists with a wealth of new data that yield insights into early solar system processes. The stone rainfall of the Markovka (H4) chondrite, 1967 East Siberia, Russia, provides an interesting sample for detailed investigation of its content, alteration, and origin of the parent asteroid.

Geochemical data on oxygen $^{16}O/^{17}O/^{18}O$ isotope ratios supposed a close relationship of H3–H6 chondrites in contrast to L and LL types.[8] To explain this phenomenon, a number of thermochronometric and geochronological methods were involved, including retention of fission tracks and Pb–Pb ages,[9] metallographic cooling rates derived from Ni zoning in Fe–Ni alloys,[10] opx–cpx, and other thermobarometers.[11] These studies of the thermal evolution of H chondrites were based on determination of two main parameters: (1) the distribution of metamorphic peak and closure temperatures for the various petrologic types, as inferred from mineralogy, and (2) cooling rates. The correlation between these parameters is not obvious, mainly due to disagreement between estimated values of the various cooling rates. A simple "onion-shell" model[12] for internally heated (i.e., due to radioactive decay of $^{26}Al \rightarrow {}^{26}Mg + \beta$) chondrite parent bodies should produce an inverse correlation, that is, slow cooling in the deep interior for higher petrologic types H5 and H6 and more rapid cooling near the periphery for lower petrologic types H3 and H4. However, it was noted that for some cases, there appears to be no correlation between the metallographic data, two-pyroxene thermometry, and petrologic type. Therefore, a

"metamorphosed-planetesimal" model was developed to resolve this discrepancy. In this model, heating occurs in small objects that are subsequently randomly accreted into larger parent bodies.[13]

It is worth noting that the rheology of asteroids differs from planets—these are rigid pieces of rock compressed by their own gravity. To date, important updates were obtained on the topography and the gravity of asteroids as from the asteroids belt (Vesta and Ceres) and as of the near-Earth families (Eros and Ryugu). These data show asteroids as coherent, but heavily fractured objects with the mean density of between 2 and 3 g/cm^3 indicating a stony composition, like chondrites, with significant porosity. Thus, the well-understood theory of gravitational potential can be used to calculate elastic deformations and stresses (σ_{ij}) of a small spherical body with a radius R[14]:

$$\partial\sigma_{rr}/\partial r + 2(\sigma_{rr} - \sigma_{\theta\theta})/r = -\rho \cdot g \cdot r/R, \sigma_{\theta\theta} = \sigma_{\varphi\varphi}, \quad (1)$$

where r is the radial distance from the bodies center at the spherical reference system (r, θ, and φ), ρ is the bodies mean density, $g = 4/3\pi \cdot \rho \cdot G \cdot R$ is the gravity acceleration on the surface, and G is the gravity constant. Spherically symmetric solution of (1) for the components of the stress tensor, $\sigma_{rr}(r)$ and $\sigma_{\theta\theta}(r)$, provides total pressure at bodies center at $r = 0$ as

$$\begin{aligned}\sigma(0) &= \sigma_{rr}(0) + \sigma_{\theta\theta}(0) + \sigma_{\varphi\varphi}(0) \\ &= 3/10 \cdot \rho \cdot g \cdot R \cdot (3 - \nu)/(1 - \nu),\end{aligned} \quad (2)$$

where ν is the Poisson elasticity coefficient with the mean value of between 0.15 and 0.25 for chondrites.[15]

Knowing the pressure and temperature margins in the interior of the parent body of the asteroid will allow us to constrain the possible phase transitions and the presence of polymorph minerals. In this paper, we analyze a composition of the Markovka (H4) chondrite by Raman microspectroscopy, a nondestructive analytical technique, providing complementary, spatially resolved data to chemical analysis. We show what kind of information concerning parent asteroids genesis and evolution can be derived by Raman spectroscopy.

2 | METHODS

2.1 | Sample preparation and characterization

The small fragment of the Markovka chondrite (H4) with dimensions about 3 × 2 × 2 cm^3 (see Figure 1), used in this work, is a part of the large meteorite fall in 1967 near Markovka Village, East Siberia, Russia. The fall was a stone rain with fragmented chondrite bodies, with the typical sizes up to 1 m, which was collected and is currently stored in the meteorite collection of the Russian Academy of Sciences (see for details official reference at Meteoritic Bulletin[16]).

FIGURE 1 Markovka (H4) chondrite fragment [Colour figure can be viewed at wileyonlinelibrary.com]

A fresh cut plate with the size ~1 × 1 cm^2 was used for the investigations.

2.2 | Scanning electron microscopy with energy-dispersive X-ray spectroscopy

Chemical composition of the samples was determined by a combination of scanning electron microscopy (SEM) and energy-dispersive X-ray spectroscopy (EDX) microanalyses. Leo Supra 50VP microscope equipped with Oxford Instruments X-Max Detector from Analytical Centre, Moscow State University, was used. Measurement parameters of the microscope system during analysis were low-pressure (40 Pa) N_2 atmosphere, 15-kV electron beam with a working distance of 7 nm, VPSE (Microscopy Variable Pressure Secondary Electron) detector, and magnifications from 200× to 2500×. The X-ray microanalysis was done by taking the EDX spectra from the selected areas and by mapping of the sample area. Identification and quantification of the elements were done after ZAF correction (the corrections of the X-ray intensities against those from a standard specimen in order to eliminate changes caused by the atomic number Z, the absorption A, and the fluorescence excitation F). Maps of the main elements allowed us to identify minerals/metal alloys and simplify subsequent spectroscopic analysis (see Figure 2).

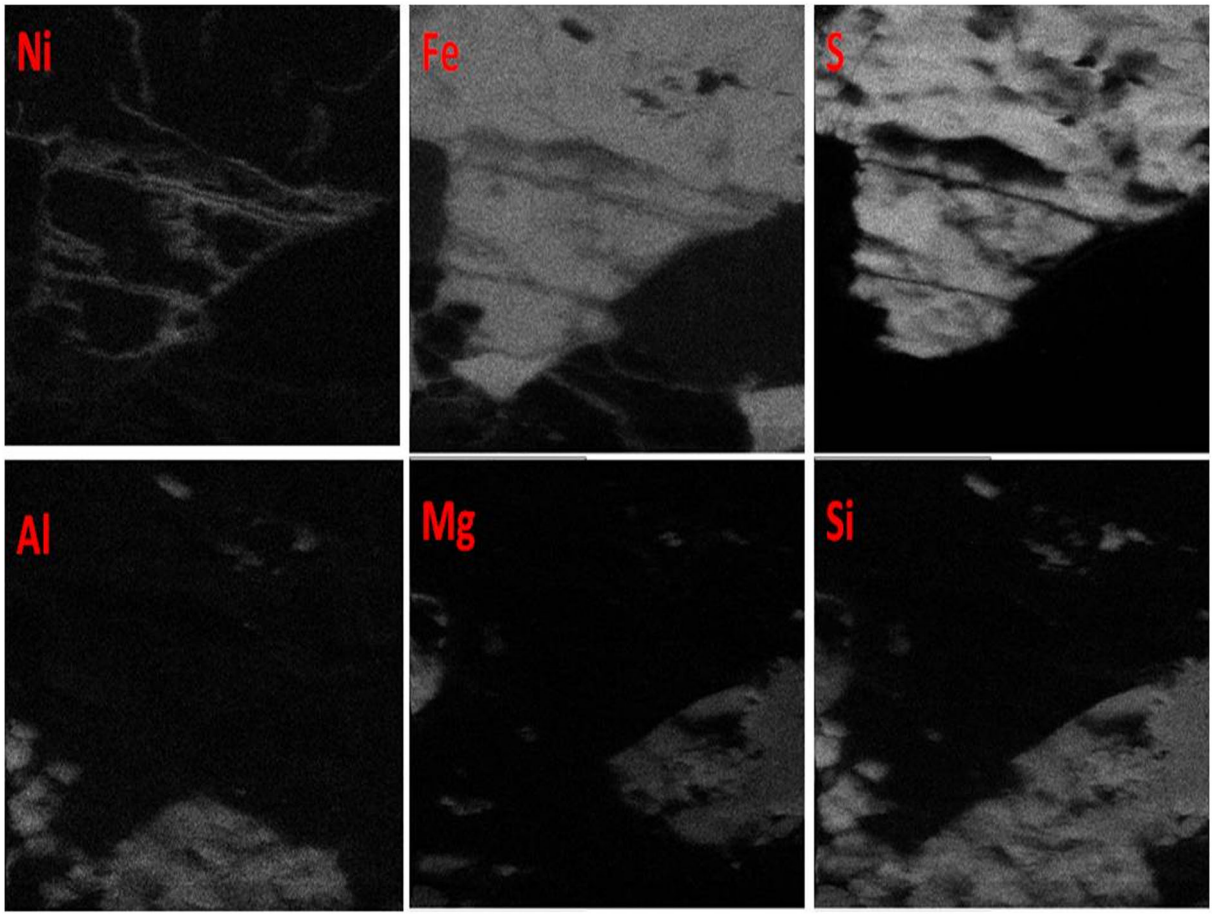

FIGURE 2 Examples of SEM–EDX maps with Ni, Fe, S, Al, Mg, and Si for troilite Fe(Ni)S (top row) and for plagioclase $Na(Ca)AlSi_2O_8$ (down row) [Colour figure can be viewed at wileyonlinelibrary.com]

TABLE 1 Chemical composition of main minerals' groups in the Markovka meteorite, as from SEM–EDX analysis

	Composition (wt%)								
Mineral group	**MgO**	**Al_2O_3**	**SiO_2**	**Na_2O**	**P_2O_5**	**CaO**	**K_2O**	**FeO**	**#Mg–#Fe–#Ca X * 100/(Mg + Fe + Ca)**
Olivine	42.51	0.03	39.86	0	0	0.03	0	18.15	80–20–0
	42.58	0.04	39.77	0.06	0.34	0.02	0	18.01	80–20–0
Pyroxene	30.59	0.17	57.13	0.02	0.35	0.85	0.01	11.84	82–16–2
	30.92	0.15	57.37	0.02	0.35	0.72	0.01	11.41	81–17–2
Plagioclase	0.09	22.32	67.84	10.34	0	2.51	0.98	0.69	$An_{12}Ab_{84}Or_4$
	0.01	22.04	63.56	9.26	0.35	2.38	0.95	2.62	$An_{12}Ab_{82}Or_6$

Quantitative chemical data are possible with accuracy till of 0.01 wt%. Typical values for the main groups of minerals are presented in Table 1.

Silicates (olivine and pyroxene), plagioclase (albitic low-Ca composition), Fe hydroxides, FeS (troilite), and FeNi alloys were recognized.

2.3 | Raman spectroscopy

Raman spectra of the Markovka meteorite were collected at the Raman laboratory of the Institute of Planetary Research at DLR Berlin using a Witec Alpha 300 System Raman microscope spectrometer equipped with a

532-nm Nd:YAG laser and a 10× objective for Raman scattered light acquisition (see Kaeter et al.[7] for details).

In order to avoid a heat-related alteration of sensitive iron-containing mineral phases, Raman spectra were taken at reduced laser powers and in vacuum ($\sim 10^{-5}$ mbar). For this, the Markovka sample was mounted inside a vacuum chamber placed on a 2D movable scanning table under the Raman microscope. The spectra were recorded at room temperature in back-scattering geometry in the Stokes shifted range from 100 to 3200 rel. cm^{-1} with a spectral resolution of approximately 4 cm^{-1}. The power of the laser was varied in the range of 0.3–3 mW with a focal spot on the sample of about 1.5 μm. We started from the lower power at each new location first, in order to avoid potential thermal effects. As far as mineral phases were recognized, the laser power was increased step by step and spectra were taken at 1 and 3 mW, for comparison. The spectrometer was wavelength calibrated using a neon lamp, and the Stokes shift was linked to the optical phonon in a silicon sample (521 cm^{-1}). Peak positions of the Raman lines were found by the least squares regression method using the Witec evaluation software.

Raman spectra of minerals can be affected by the impurities imposed by the thermal diffusion and geochemical substitution of elements. The reference spectra of several standard mineral classes, such as olivine, pyroxene, and plagioclase, were collected for direct comparison and stored in databases.

The choice of the sampling areas was made by intuitive search for the places with various optical contrasts as well as at several randomly selected positions. In all these places, test spectra were taken and served to a final decision of the point-to-point measurements, and linear and area scans (Figure 3). Area scans were made in vicinity of detected characteristic phases, to show the phase distribution maps. Linear scans were taken to accurately show the areas crossing several phases in order to further separation and verification of the strongly mixed phase cases. Point measurements were made where a sole phase or a few phase mixture was found by the rapid test search.

Three linear scans of 275-, 295-, and 280-μm total length, respectively, with 50 steps per scan, and according step size of around 6 μm were performed to cross a couple of characteristic areas. The area scan comprises an area of 300 × 300 μm with 75 × 75 measurement points with a step size of 4 μm. The measurement time was 10-s integration time per point. This allowed fast determination of major mineral phases in the sample: silicates (olivine and pyroxene), plagioclase, and iron oxide.

3 | RESULTS AND DISCUSSION

Spectra at different locations on the meteorite are commonly (at a very few exceptions) from a few phases (Figure 4). Admixing of mineral phases results in the broadening of characteristic vibration bands and

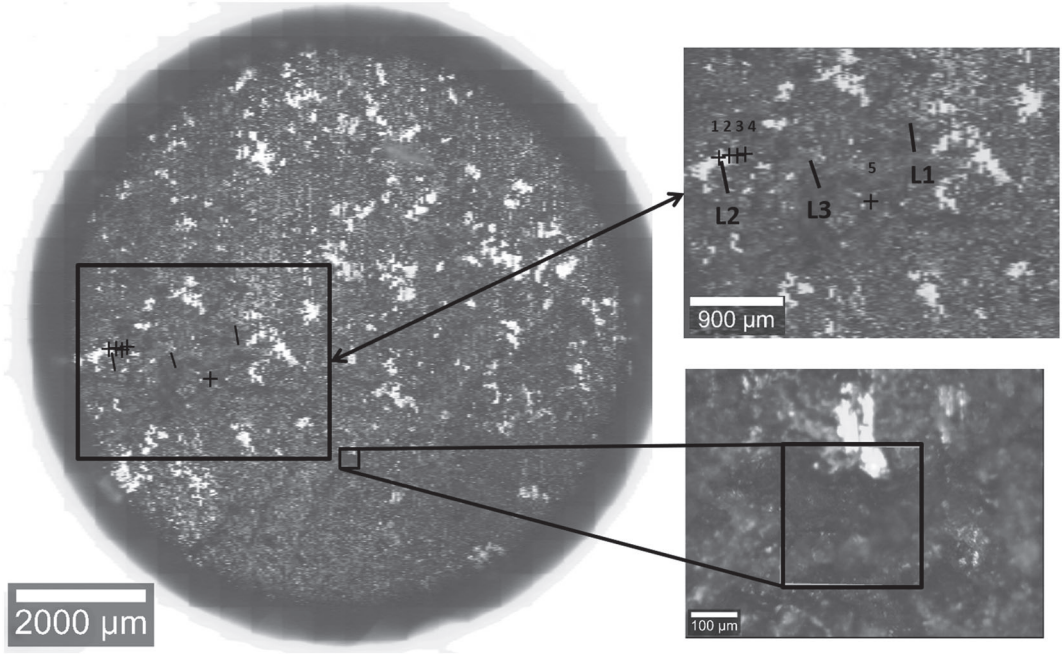

FIGURE 3 General view of the investigated regions on the Markovka meteorite sample. Left: Image of ∅ 9-mm area taken through the optical path of the Raman microscope. Right upper plot: Enlargements of the investigated areas with the positions of single-point measurements, line (L) scans. Right lower microscopic image: Enlargement of the investigated area with area scan

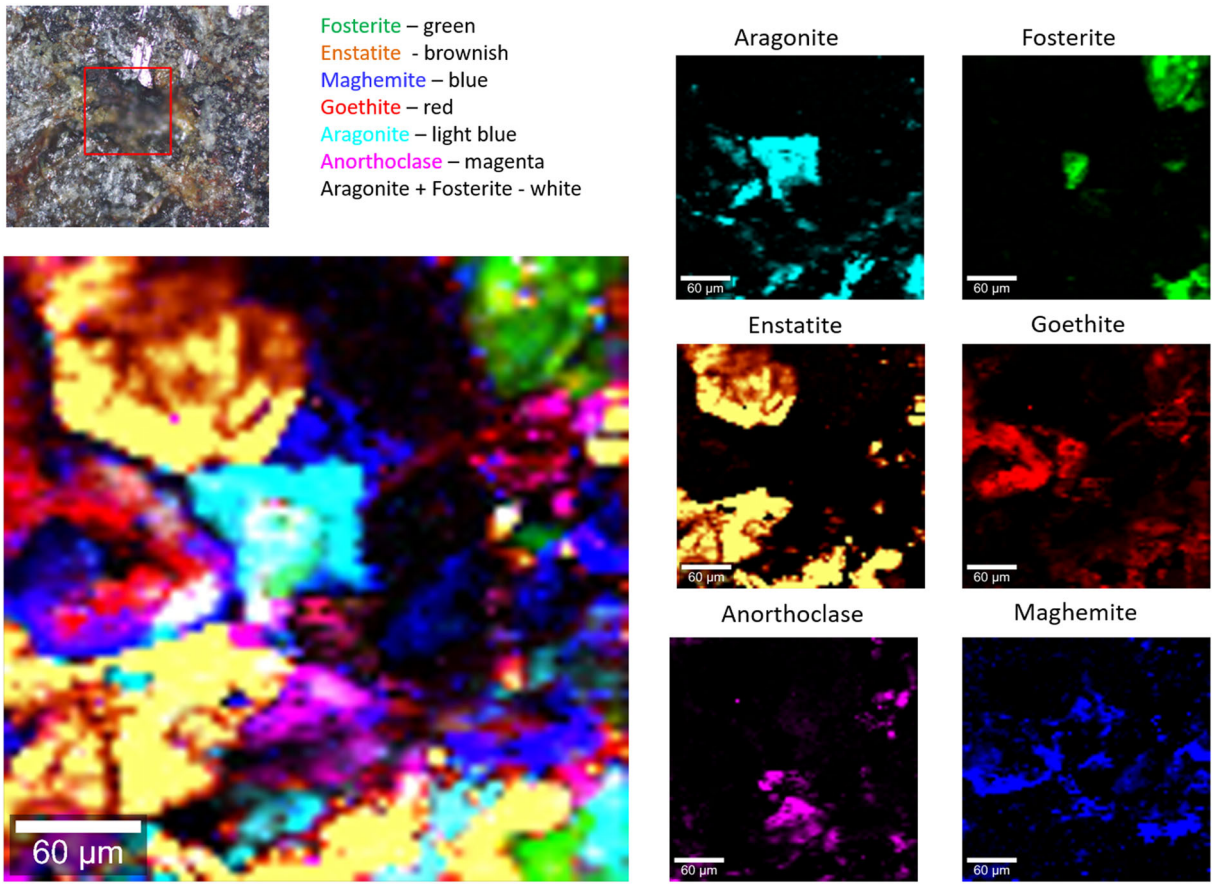

FIGURE 4 Maps of the mineral phases in the Markovka meteorite confirmed by Raman spectroscopy. Upper left: Image of the selected area taken by the optical Olympus microscope. Lower left: Color composite of mineral phases in the selected area. Right: Color-coded maps of individual mineral phases [Colour figure can be viewed at wileyonlinelibrary.com]

common lowering of magnitudes, known for highly inhomogeneous samples such as meteorites.

Three "optically" different regions (indicated as L1, L2, and L3 in Figure 3) were selected. The mineral phases found in the Markovka meteorite fragment by Raman spectroscopy are presented in Figure 4.

3.1 | Silicates

Silicates are the most abundant mineral class and spread over entire area in the meteorite (see Figure 4). They are presented mainly by orthosilicates ($[SiO_4]^{4-}$) olivine and inosilicates ($[Si_nO_{3n}]^{2n-}$) pyroxene groups.

The olivine spectra are dominated by the SiO_4 tetrahedra internal stretching (ν_1, ν_3: 820–960 cm^{-1}) and bending (ν_2, ν_4: 400–610 cm^{-1}) modes, with most strong transitions for the stretching modes, used for general classification of olivines. The stretching modes ν_{AS} (Si–O asymmetric stretching, $(\nu_1 + \nu_3)_{AS}$) and ν_{SS} (Si–O symmetric stretching $(\nu_1 + \nu_3)_{SS}$) exhibit a constant energy difference $\nu_{AS} - \nu_{SS} = 32\ cm^{-1}$ in the recorded spectra presenting olivines. The modes peak at $\nu_{AS} = 854\ cm^{-1}$ and $\nu_{SS} = 822\ cm^{-1}$, which classifies the observed olivines to an average composition of Fa_{20} Fo_{80}: Fo values (Fo = Mg/(Mg + Fe) in a mole, were obtained using the calibration,[17] which is in a very good relation to the -SEM–EDX data (Table 1). Both mentioned values indicate a Mn-poor forsterite, otherwise increasing the intermode energy spacing.[18] The same arguments exclude significant abundances of Co–olivine and Ni–olivine in the investigated areas on a meteorite. Detailed SEM–EDX analysis of Markovka olivine provides the following composition (in wt%): Mn—0.03, Co—0.012, and Ni—0.012.

With the accuracy of used spectral resolution, we cannot be confident on the partial occurrence of Ca in the M2 site of olivines that could be potentially linked to a minor blue shift (not exceeding 4 cm^{-1}) of the SiO_4 stretching modes. This assumption however cannot be unambiguously confirmed by the low-energy part of the olivine spectra at different locations (Figure 5), where the lines are rather pure olivine or mixed with other phases. For instance, the line at 214 cm^{-1}

(Point 4, Figure 4) can be assigned both to a $T(SiO_4)$ translation A_g mode of forsterite (Mg_{80}, $Fe_{20})_2SO_4$ and to a $T(SiO_4)$ B_{3g} mode of monticellite ($CaMgSiO_4$).[19]

We note that alone olivine component (within the scale of the diagnostic laser spot, 1.5 μm) was found only at a few exclusive locations (e.g., Point 4 in Figure 5). In this case, we could safely increase the excitation intensity in order to resolve weaker lines in the low-energy part of the spectrum. Beside the internal SiO_4 modes, only the characteristic for a Si–O bond, vibration modes were observed in this case: a $T(SiO_4)$ translation mode and a mixed $M2 + R(SiO_4)$ translation + libration mode at 222 and 314 cm^{-1}, respectively (mode assignment as from Chopelas[19]). No characteristic cation (M)-related vibration modes, such as M-oxygen bond modes at below 500 cm^{-1}, were resolved in the strongly overlapped spectra and cannot be used for justification of possible occurrence of low Ca or trace transition metals in the olivine molecule sites.

Mixed spectra of a few mineral phases were often presented in the Raman spectra (Points 2 and 3 in Figure 5). Two specific bands lying between 450 and 515 cm^{-1} in the Raman spectrum at Position 2 (Figure 5) indicate admixed tectosilicates with typical ring-breathing $RB(SiO_4)$ modes of the four-membered rings of tetrahedra, whereas the strongest band peaked at 510 cm^{-1} is typical for feldspar group with a four-membered ring.[20] The characteristic set of $RB(SiO_4)$ modes: (weak 455, 480, and 510 cm^{-1}) constrains the classification of this feldspar to high-temperature plagioclase group ($(Ca, Na)(Al, Si)_4O_8$), whereas the lowest energy cage-shear band (150–200 cm^{-1}) has a peak at about 169 cm^{-1}, right between the values for oligoclase (161 cm^{-1}, Na/(Ca + Na) ranges from 70% to 90%) and andesine (177 cm^{-1}, Ca/(Ca + Na) is between 30% and 50%).[20]

The next abundant silicate phase, found in the investigated sample, is pyroxene (Figure 6, top). Structurally, pyroxene is presented as individual grains and cement between grains of olivine. In the grains, the Raman spectra exhibit a range of characteristic Mg–Fe orthopyroxene (opx) series—enstatite (En: $MgSiO_3$) to ferrosilite (Fs: $FeSiO_3$). It is known that for the opx series at H chondrites, the characteristic Raman spectral regions are 850–1050 cm^{-1} (ν(Si–O_{nb}) stretching modes), 630–750 (ν(Si–O_b–Si) bending modes), and weaker ν(O–Si–O) bend bands at 500–600 cm^{-1}, where O_{nb} and O_b stand for nonbonded oxygen and the chain-bonded oxygen of the SiO_4 tetrahedron of inosilicates, respectively.[21]

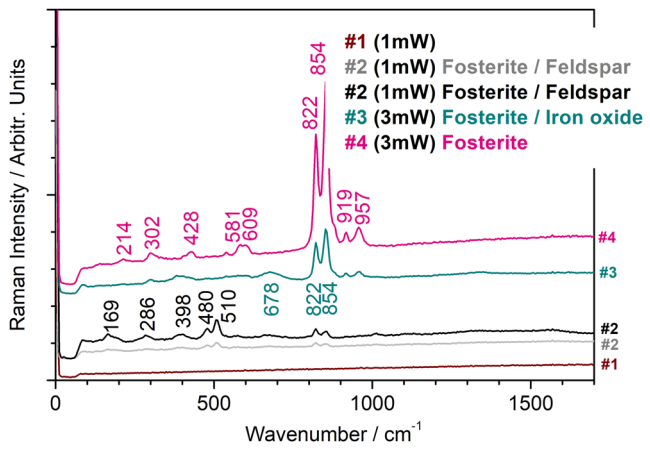

FIGURE 5 Raman spectra of the Markovka meteorite at different locations #1–4 with common olivine abundance (characteristic lines at >822 cm^{-1}). The laser power at positions #1 and #2 was ~1 mW and at positions #3 and #4 was ~3 mW. Spectra at positions #2 are identical and differ only in intensities of the observed bands. Spectra are shifted vertically for the better viewing [Colour figure can be viewed at wileyonlinelibrary.com]

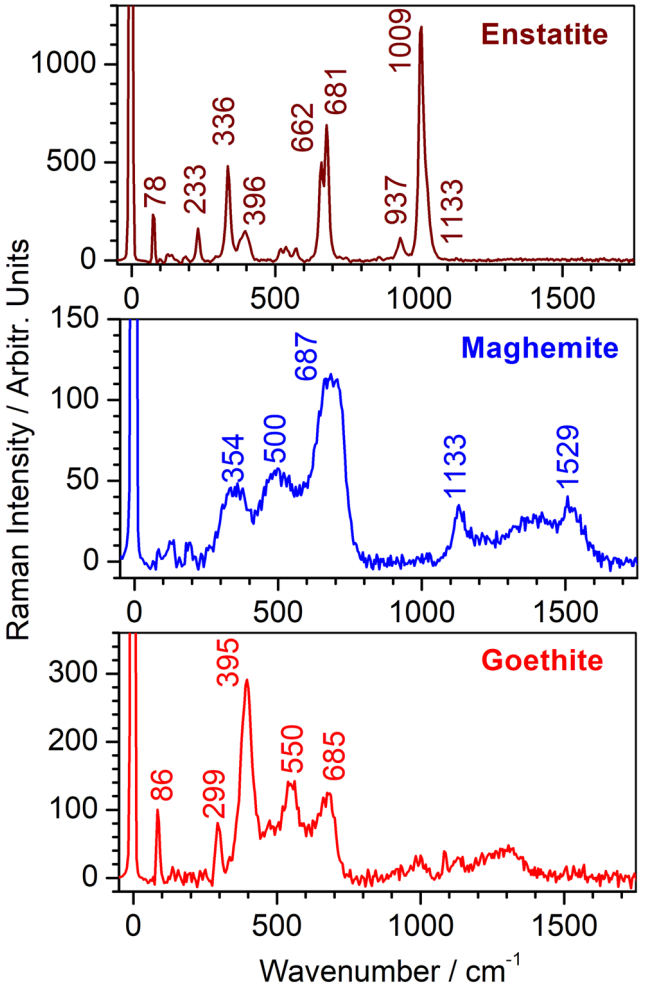

FIGURE 6 Typical pyroxene (top graph) and iron oxides in the Raman spectra of the Markovka sample [Colour figure can be viewed at wileyonlinelibrary.com]

The low-energy broad bands can be attributed to lattice vibration modes: a metal (M)–O stretch to those with peaks at about 233 and 336 cm^{-1} and a Mg–O stretch to those with a peak at about 396 cm^{-1}. The line set of 1009, 662/683, and 336 cm^{-1} of the Markovka sample (enstatite, Figure 6, top) allows to constrain a low-Ca composition of $En_{82}Fs_{16}Wo_2$, using calibrations of these lines from Wang et al.[21] This fits well to the SEM–EDX data. Virtually constant Fo and Fs contents in both low-Ca pyroxene and olivine indicate the equilibrated grains experienced medium thermal metamorphism. Thus, Mg, Fe, and Ca partitioning between minerals has progressed almost to completion.

3.2 | Iron oxides and oxyhydroxides

Spectral features of maghemite (γ-Fe_2O_3) (Figure 6, middle) have been found in several scans. Magnetite (Fe_3O_4) is known to undergo the following phase transitions with temperature increase.[22]

$$Fe_3O_4 \rightarrow \gamma - Fe_2O_3\ (200^\circ C) \rightarrow \alpha - Fe_2O_3\ (400^\circ C),$$

where maghemite (γ-Fe_2O_3) is transformed to hematite (α-Fe_2O_3) starting at about 400°C. Because any evidence of hematite was found in the Raman spectra of the samples (see Figure 6, top), we suppose that the maximum temperature of the Markovka parent body did not exceed 400°C. It provides important physical constraint on the model of its evolution.

Despite small differences in the Stokes line peak positions (within ±5 cm^{-1}), there is good agreement in the reported spectra of goethite (α-FeOOH) with the observed broad spectral bands centered at about 299, 395, 479, 550, and 685 cm^{-1}[[23]] (see Figure 6, bottom). The Raman spectrum of lepidocrocite (γ-FeOOH) has also been extensively investigated, and there is a consensus on the most important peaks of 245, 373, and 493 cm^{-1} (shoulder) and 522 and 650 cm^{-1} (shoulder).[24]

Lepidocrocite is formed in the weathering crusts of basic and ultramafic rocks, and oxidation zones (iron hats) as a result of hydrolysis of Fe-containing minerals during a hydrothermal low-temperature process. These lines were not detected in the Markovka sample, and it is an indication of weak ground contamination.

3.3 | Aragonite

Most remarkable in the Markovka (H4) meteorite is the finding of carbonates—namely, aragonite ($CaCO_3$) (Figure 7). Carbonate minerals are typical for the CM

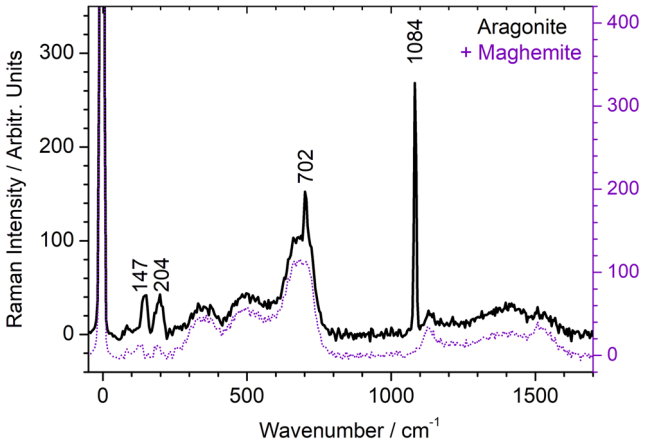

FIGURE 7 Discrete line of aragonite in the Raman spectra of the Markovka sample, occurred with admixed maghemite. The maghemite spectrum, characterized with broad Raman bands, is shown in the background for a comparison [Colour figure can be viewed at wileyonlinelibrary.com]

group carbonaceous chondrite meteorites, along with silicates and sulfides, with which they are intergrown.[25] Widely accepted, CM carbonaceous chondrites were altered from their original anhydrous mineralogy by aqueous fluids shortly after parent body accretion. But H chondrites are dry and have low carbon content, usually.

Two well-known carbonate polymorphs, calcite (trigonal structure, R-3c) and aragonite (orthorhombic structure, Pmcn), have similar lines in the spectrum caused by the symmetric CO_3 stretching mode (1086 and 1084 cm^{-1}, respectively). A significant difference is noticeable for the low-frequency oscillation modes that are more sensitive to structural changes: 282 cm^{-1} for calcite and 204 cm^{-1} for aragonite.[26] The vibrational bending modes also differ: the doublet characteristic of aragonite at 702 cm^{-1} is visible in the Raman spectrum of the Markovka (see Figure 7).

For the Earth geology, aragonite is usually indicative for the blueschist metamorphic conditions for which the range in the peak temperature is ~200–350°C and the pressure is ~700 MPa.[27] Using the overall transformation rate of aragonite to calcite, the partial transformation of aragonite to calcite was explored to constrain *P–T–t* paths for rocks metamorphosed at convergent plate junction (see Figure 8).

In the study of Liu et al.,[28] a series of Raman experiments on the phase transition of calcite at high pressure and high temperature were carried out using a hydrothermal diamond anvil cell. It was found that calcite I transformed into calcite II and calcite III at pressures of 1.62 and 2.12 GPa and room temperature. With increasing temperature, the phase transition of calcite III into aragonite occurred. Aragonite was retained upon slowly

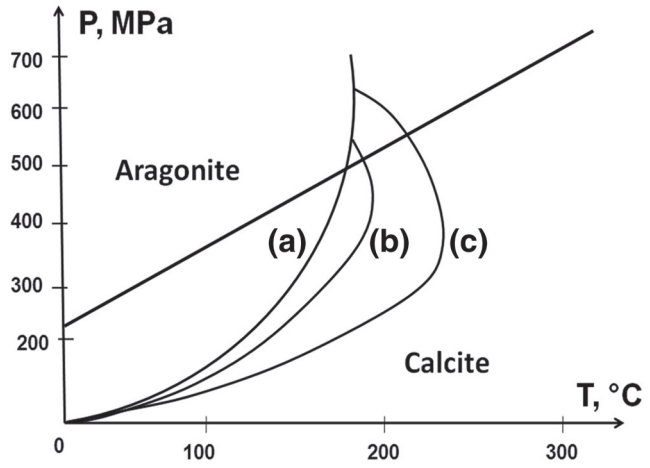

FIGURE 8 Selected *P–T* trajectories for uplift paths of aragonite-bearing rocks from blueschist facies metamorphism. The aragonite/calcite phase boundary is shown by a bold line. Curves (a), (b), and (c) are possible cooling and uplift paths for Franciscan rock under different conditions (uplift rates ~1–3 mm/year, initial depth ~20–30 km), according to Liu and Yund[27]

cooling of the system, indicating that the transition of calcite III into aragonite was irreversible. Kinetics of calcite–aragonite transformation to a first-order approximation may be estimated from a time dependence of electrical bulk resistance.[29] For example, at 2.5 GPa and 780°C, the characteristic transformation time is ~7.5 h, at 2 GPa, and 735°C ~33 h. So, aragonite, as a high-pressure polymorph of calcite, could be stable for a long time at pressure starting 200 MPa and low temperature.

4 | CONCLUSIONS

Raman data of the Markovka (H4) meteorite provide a basis for new unexpected constraints for both main models of an H-chondrite parent asteroid. For the "onion-shell" model, size of the body, accepted for calculations, remains under question. So, aragonite as a high-pressure carbonate polymorph could be formed from calcite during a strong impact followed by quenching. With a mean density of chondrites as 3–4 g/cm^3, pressure of 200 MPa at body with a radius ~300 km is possible, according to Equation (2). Theoretically, aragonite could be preserved in a parent body of this size until its destruction. But, current accretion models suppose a quite short time interval of ~1–2 million years (since Ca–Al inclusions formation) and planetesimals with a preferential size of ~50–200 km in radius.[30] And, for this option, Markovka does not contain essential impact melt (see Figure 1), and the structure of olivine in chondrules is typical for S0–S1 degree of the shock metamorphism.

The "metamorphosed-planetesimal" model is more likely, assuming that aragonite was deposited from a Mg-rich solution, like hydro-alteration by CM carbonaceous chondrites.[25] In this case, the question about the possible water source arises. If these were grains of water ice, then early migration of the Markovka parent body to the "snow line" was necessary. So, Raman map on Figure 4 reveals asteroid aqueous alteration by cementation of pores produced by the melting of tens of micrometer-size particles of H_2O-rich ice. Also, presented Raman data concerning maghemite confirm this possibility: the presence of ice due to the latent heat of melting could significantly lower the overall temperature.

In the example of Markovka (H4), we can see as chondrite meteorites store the keys on evolution processes at the early solar system. Raman spectroscopy provides additional unique possibilities for their chemical and mineralogical analysis.

ACKNOWLEDGEMENTS

The study was supported by the grant from the Russian Science Foundation 21-17-00120, https://rscf.ru/project/21-17-00120. We acknowledge the access to Raman laboratory of the DLR Institute of Planetary Research in Berlin.

ORCID

Sergey Voropaev https://orcid.org/0000-0001-8259-5359
Ute Böttger https://orcid.org/0000-0003-2266-7271

REFERENCES

[1] J. T. Wasson, *Meteorites: Their Record of Early Solar System History*, Freeman & Co., New York **1985**.
[2] G. R. Huss, A. E. Rubin, J. N. Grossman, Thermal metamorphism in chondrites, in *Meteorites and the Early Solar System II*, (Eds: D. S. Lauretta, H. Y. McSween Jr.) Space Science Series, University of Arizona Press, Tucson, Arizona, USA **2006**, p. 567.
[3] L. Pittarello, K. Baert, V. Debaille, P. Claeys, *Meteorit. Planet. Sci.* **2015**, *50*, 1718.
[4] L. Bonal, E. Quirico, L. Flandinet, G. Montagnac, *Geochim. Cosmochim. Acta* **2016**, *189*, 312.
[5] B. J. Saikia, G. Parthasarathy, R. R. Borah, R. Borthakur, A. J. D. Sarmah, *J. Astrophys. Aerospace Technol.* **2017**, *5*, 100149.
[6] A. Wesełucha-Birczyńska, M. Zmudzka, *J. Mol. Struct.* **2008**, *887*, 253.
[7] D. Kaeter, M. A. Ziemann, U. Böttger, I. Weber, L. Hecht, S. A. Voropaev, A. V. Korochantsev, A. V. Kocherov, *Meteorit. Planet. Sci.* **2018**, *53*, 416.
[8] R. N. Clayton, *Annu. Rev. Earth Planet. Sci.* **1993**, *21*, 115.
[9] P. Pellas, D. Storzer, *Proc. R. Soc. London* **1981**, *374*, 253.
[10] E. R. D. Scott, R. S. Rajan, *Geochim. Cosmochim. Acta* **1981**, *45*, 53.
[11] H. Y. McSween, A. D. Patchen, *Meteoritics* **1989**, *24*, 219.

[12] M. Trieloff, E. K. Jesserberger, I. Herrwerth, J. Hopp, C. Fiehnl, M. Gherlls, M. Bourot-Denise, P. Pellas, *Nature* **2003**, *422*, 502.
[13] E. R. D. Scott, 66th Annual Meteoritical Society Meeting. **2003**; Contribution #5293.
[14] L. Landau, E. Lifshitz, Theoretical physics, in *Theory of Elasticity*, Vol. 7, Nauka, Moscow **1987** 245.
[15] S. A. Voropaev, A. V. Kocherov, C. A. Lorenz, A. V. Korochantsev, N. V. Dushenko, D. M. Kuzina, I. I. Nugmanov, Y. Jianguo, *Dokl. Phys.* **2017**, *62*, 486.
[16] Meteoritic Bulletin. https://www.lpi.usra.edu/meteor/metbull.php?sea=Markovka&sfor=names
[17] K. E. Kuebler, B. L. Jollif, A. Wang, L. A. Haskin, *Geochim. Cosmochim. Acta* **2006**, *70*, 6201.
[18] T. Mouri, M. Enami, *J. Mineral. Petrol. Sci.* **2008**, *2*, 100.
[19] A. Chopelas, *Am. Mineral.* **1991**, *76*, 1101.
[20] J. J. Freeman, A. Wang, K. E. Kuebler, B. L. Jolliff, L. A. Haskin, *Can. Mineral.* **2008**, *46*, 1477.
[21] A. Wang, B. Jolliff, L. Haskin, K. Kuebler, K. Viskupic, *Am. Mineral.* **2001**, *86*, 790.
[22] F. E. De Boer, P. W. Selwood, *J. Am. Chem. Soc.* **1954**, *76*, 3365.
[23] D. L. A. de Faria, S. V. Silva, M. T. de Oliveira, *J. Raman Spectrosc.* **1997**, *28*, 873.
[24] M. Hanesch, *Geophys. J. Int.* **2009**, *177*, 941.
[25] M. R. Lee, P. Lindgren, M. R. Sofe, *Geochim. Cosmochim. Acta* **2014**, *144*, 126.
[26] F. Rull, J. Martinez-Frias, A. Sansano, J. Medina, H. G. M. Edwards, *J. Raman Spectrosc.* **2004**, *35*, 497.
[27] M. Liu, R. A. Yund, *Contrib. Mineral. Petrol.* **1993**, *114*, 465.
[28] C. Liu, H. Zheng, D. Wang, *High Pressure Res.* **2017**, *37*, 545.
[29] N. Bagdassarov, A. Slutskii, *Phase Transit.* **2003**, *76*, 1015.
[30] E. Chiang, A. Youdin, *Annu. Rev. Earth Planet. Sci.* **2010**, *38*, 493.

How to cite this article: S. Voropaev, U. Böttger, S. G. Pavlov, F. Hanke, D. Petukhov, *J Raman Spectrosc* **2021**, 1. https://doi.org/10.1002/jrs.6147